INDEPENDENT OPTICAL NAVIGATION PROCESSING FOR THE OSIRIS-REX MISSION USING THE GODDARD IMAGE ANALYSIS AND NAVIGATION TOOL

Andrew Liounis[1*], Jason Swenson[1], Jeffrey Small[2], Josh Lyzhoft[1], Benjamin Ashman[1], Kenneth Getzandanner[1], Dolan Highsmith[2], Michael Moreau[1], Coralie Adam[3], Peter Antreasian[3], and Dante S. Lauretta[4] [1]NASA Goddard Spaceflight Center, 8800 Greenbelt Rd., Greenbelt, MD 20771 [2]The Aerospace Corporation, 14745 Lee Rd, Chantilly, VA 20151 [3]KinetX Space Flight Dynamics Practice, 21 West Easy Street, Simi Valley, CA 93065 [4]Lunar and Planetary Laboratory, University of Arizona, 1415 N 6th Ave, Tucson, AZ 85705 [*][andrew.j.liounis@nasa.gov]

Abstract. *The OSIRIS-REx mission to the asteroid (101955) Bennu heavily relies on optical navigation to provide relative state information between the asteroid and the spacecraft. These measurements enable determination of the spacecraft's orbit to the tight requirements needed to meet the science goals of the mission. In this document we describe the algorithms and techniques used by the Goddard independent verification and validation navigation effort to extract these measurements from the images taken by the spacecraft during the mission. We also demonstrate the capabilities of the techniques by showing the high accuracy of the results when used in an orbit determination solution.*

Introduction. The OSIRIS-REx mission to the asteroid (101955) Bennu is uniquely challenging from the navigation perspective. Due to the low-gravity environment, non-gravitational forces play a dominant role in the dynamics of the spacecraft, and science goals require ultra-precise knowledge of the spacecraft's location at all times.[1] The combination of these factors means that ground-based radiometric tracking is not sufficient on its own to successfully navigate the spacecraft, and direct measurements of the relative state between the asteroid and the spacecraft are required. For OSIRIS-REx, these measurements take the form of optical navigation (OpNav) measurements.

Due to the unique challenges of the mission, the OSIRIS-REx Flight Dynamics team is organized into a prime and an independent verification and validation (IV&V) navigation team. The prime team provides official navigation products to the project and is largely composed of KinetX Aerospace Engineers. The IV&V team largely provides independent assessments of the navigation performance and products, along with providing surge support to the prime team, and is largely comprised of engineers from NASA's Goddard Space Flight Center and The Aerospace Corporation.

One of the main tasks of the IV&V flight dynamics team is to provide independent orbit determination (OD) to compare with the prime products. To ensure the OD is as independent as possible, the IV&V team generates their own OpNav products using the Goddard Image Analysis and Navigation Tool (GIANT) developed by the IV&V team and the stereophotoclinometry (SPC) software suite developed by Dr. Robert Gaskell.[2]

In this document we detail the algorithms used in the GIANT software to produce independent OpNav measurements. We provide an overview of all of the algorithms used in the software, while devoting particular attention to novel techniques and algorithms. To conclude we also provide a sample of results generated using GIANT and show their performance in the independent OD performed by the IV&V team.

Camera Calibration and Attitude Estimation. At its essence, OpNav relates lines of sight from a two-dimensional image to known objects in the three-dimensional world. This requires knowledge of a precise model for mapping directions from three-dimensions onto the image plane and for mapping points on an image plane into directions in three-dimensions. It also requires knowledge of how the camera is oriented with respect to the three-dimensional world beyond what is typically achievable by relying solely on the knowledge of the spacecraft's attitude from the attitude subsystem. Both of these requirements can be met by matching observations of star fields with a catalogue of known star locations in the three-dimensional world.

In GIANT, this matching is handled in two distinct steps. First, the image is processed to identify candidate sub-pixel star locations in the field of view through the application of image processing techniques.[3] Next, these candidate star locations are matched with catalogue records using a random sampling and consensus (RANSAC) algorithm.[4] Once the matching has been performed, the image-catalogue pairs can be used to estimate the attitude, the camera model, or both.[5] The following subsections describe these steps in further detail.

Identifying Potential Stars in an Optical Image. GIANT first finds all of the candidate points in the image that may be star observations. This is done through pure image processing, assuming no *a priori* knowledge of what stars are expected to be in the image or where to expect them. GIANT largely follows the image processing steps described in Ref. [3] and we briefly describe them here with specific attention to notable deviations.

The first step in the image processing is to remove some of the background light from the image by flattening the image. Generally, this is done by subtracting a 5×5 median filtered version of the image from the original image.[3] In some cases, however, additional back-

ground light must be removed beyond what is removed through the median filter flattening. This is done by estimating a linear gradient change over small regions of the image and subtracting the estimated gradient from the original image [6, in review].

The next step is to threshold the flattened image to identify points that have a high signal-to-noise ratio. The noise for the image can be approximated in three different ways through computing statistics on (A) a random sampling of the pixels in the image,[3] (B) an active region of the detector that is not exposed to light, or (C) a local region of the image. Regardless of how the noise level is calculated, the flattened image is divided by the standard deviation to give the rough signal-to-noise ratio for each pixel. These values are then thresholded, keeping pixels with signal-to-noise ratios greater than some user-defined threshold (usually around 8).

Following the thresholding, the thresholded image is processed using a connected components algorithm to identify blobs of pixels where the signal-to-noise ratio is met.[7] Using connected components is necessary so that stars that result in multiple pixels above the signal-to-noise ratio are not considered multiple times. The blobs identified by connected components can be filtered based on the area that they cover to attempt to remove any noise spikes or extended bodies from consideration.

Each blob is processed to identify the subpixel center of the blob. This is done by fitting a general 2D Gaussian function of the form:

$$f(x,y) = Ae^{\left(-\left[a(x-x_0)^2-2b(x-x_0)(y-y_0)+c(y-y_0)^2\right]\right)} \quad (1)$$

to the DN values in the pixels containing the blob using least squares. The values for A, a, b, c, x_0, and y_0 are estimated in the least squares solution, (x, y) is the pixel pair in the image being considered, and f is the DN value for that pixel pair. The subpixel center of the blob is then (x_0, y_0). The least squares estimation can either be performed using iterative least squares, or by linearizing the fit by taking the natural logarithm of each side of Eq. (1).

The identified subpixel center of each blob is stored as a possible star location in the image and passed to the star idenfitication routines defined in the following subsection.

Matching Potential Stars with Known Stars From a Star Catalogue. With possible star locations identified in the image, a RANSAC algorithm is used to identify which points correspond to which stars taken from a star catalogue. The RANSAC algorithm used in GIANT is described in the following steps:

1. The *a priori* attitude information for each image is used to query the star catalogue for the expected stars in the field of view of each image.
2. The retrieved catalogue stars are transformed into the camera frame and projected onto the image using the *a priori* image attitude and camera model.
3. The projected catalogue locations are paired with previously identified potential star image points using a euclidean distance nearest neighbor Approach.
4. The initial pairs are thresholded based on the distance between the points, as well as for stars that are matched with 2 or more image points and image points that are close to 2 or more stars.
5. Four star pairs are randomly sampled from the set of remaining potential pairs after thresholding.
6. The sample is used to estimate a new attitude for the image.
7. The new solved-for attitude is used to re-rotate and project the queried catalogue star directions onto the image.
8. The new projected locations are compared with their matched image points and the number of inlier pairs (pairs whose distance is less than a specified threshold) are counted.
9. The number of inliers is compared to the maximum number of inliers found by any sample to this point and:
   (a) if there are more inliers using the attitude estimated from the current sample:
      - The maximum number of inliers is set to the number of inliers generated for this sample.
      - The inliers for this sample are stored as correctly identified stars.
      - The sum of the squares of the distances between the inlier pairs for this sample is stored.
   (b) if there are an equivalent number of inliers to the previous maximum number of inliers, then the sum of the squares of the distance between the pairs of inliers is compared to the sum of the squares of the previous inliers, and if the new sum of squares is less than the old sum of squares:
      - The maximum number of inliers is set to the number of inliers generated for this sample.
      - The inliers are stored as correctly identified stars.
      - The sum of the squares of the distances between the inlier pairs is stored.
10. Steps 5–9 are repeated for a specified number of iterations, and the final set of stars stored as correctly identified stars becomes the identified stars for the image.

It is also possible to skip the RANSAC and rely solely on nearest neighbors to perform the star pairing by stopping at step 4. The end result is a pairing of subpixel image points with catalogue stars that can then be used to either update the attitude for the image, or to estimate an update to the camera model used to relate directions in the camera frame to points on the image plane as described in the following subsections.

Attitude Estimation. Given a pairing between points in an image and catalogue star inertial locations, it is possible to determine the inertial pointing for an image. This is done by first converting the image points into unit vectors in the camera frame using the inverse of the camera model, and then estimating the rotation that best aligns the inertial unit vectors from the star catalogue with the unit vectors from the image in the camera frame, known as Wahba's problem:[8]

$$\min_{\mathbf{T}} J(\mathbf{T}) = \frac{1}{2}\sum_i w_i \left\|\mathbf{b}_i - \mathbf{T}\mathbf{a}_i\right\|^2 \tag{2}$$

where $\mathbf{a}_i$ are the catalogue unit vectors in the inertial frame, $\mathbf{b}_i$ are the unit vectors passing through the image pixels expressed in the camera frame, $\mathbf{T}$ is the rotation matrix to transform from the inertial frame to the camera frame, and w_i is some weight corresponding to each pair. In GIANT, this rotation is estimated using Davenport's q-Method Solution to Wahba's problem.[9] The implementation of the q-Method Solution is straightforward so the details are not presented here.

Camera Calibration. Given a pairing between points in an image and catalogue star directions in the camera frame, it is possible to estimate a camera model that projects the star locations onto the image plane, a process known as camera calibration.[10] In GIANT, the process of camera calibration is handled using a Levenberg-Marquardt iterative least squares algorithm as is done in Ref. [10]. The steps for this process are:

1. Compute the Jacobian matrix $\mathbf{J}_i = \frac{\partial \mathbf{x}_{Ii}}{\partial \mathbf{c}}$ where $\mathbf{J}_i$ is the Jacobian matrix for star direction i, $\mathbf{x}_I$ is the projected pixel location for star direction i, and $\mathbf{c}$ is a vector containing the camera model parameters being estimated using the current best estimate of the camera model for each star direction in the camera frame.

2. Compute the pre-fit residuals $\mathbf{r}_r$ between the projected star locations in the image and the observed star locations using the current best estimate of the camera model.

3. Compute the update to the camera model using $\Delta\mathbf{c} = \left(\mathbf{H}^T\mathbf{W}\mathbf{H} + \lambda \text{diag}\left(\mathbf{H}^T\mathbf{W}\mathbf{H}\right)\right)^T \mathbf{H}^T\mathbf{r}_r$ where $\mathbf{H} = \begin{bmatrix} \mathbf{J}_1 \\ \mathbf{J}_2 \\ \vdots \\ \mathbf{J}_n \end{bmatrix}$, $\mathbf{W}$ is an optional weighting matrix, and λ is the Levenberg-Marquardt parameter.[10]

4. Compute the post-fit residuals $\mathbf{r}_o$ and:
   - If $\|\mathbf{r}_r\| \approx \|\mathbf{r}_o\|$ then the fit has converged and iteration can be stopped.
   - If $\|\mathbf{r}_r\| < \|\mathbf{r}_o\|$ then the residuals are diverging and λ should be increased to $\lambda = 10 * \lambda$.
   - If $\|\mathbf{r}_r\| > \|\mathbf{r}_o\|$ then the residuals are converging and λ should be decreased to $\lambda = \lambda/10$ and $\mathbf{c}$ should be set to the estimated value.

5. Repeat steps 1–4 until convergence.

The camera models are usually initialized using manufacturer-specified values for the pixel pitch and focal length, and assuming zero distortion. Then the camera calibration process solves for the correct values for these terms. GIANT provides multiple camera models that can be estimated[11–14] and additionally provides the ability to estimate a temperature-dependent scaling as well as a residual attitude misalignment term for each image alongside the standard camera model parameters for each model.

Unresolved Optical Navigation. During the early stages of approach to an object, it frequently has an apparent diameter that is much smaller than a single pixel in the camera. This leads to the object appearing primarily as a point spread function in the image. In GIANT these point spread function–dominated observations are handled exactly the same way as stars to identify the sub-pixel center of brightness in the field of view.[15] Once the center of brightness is found, it is phase-corrected to correspond to the center-of-figure for the object. The phase correction function used is

$$\delta\mathbf{p} = \hat{\mathbf{s}} \begin{cases} 0.0062 r_p p & p < 80 \\ 0.0065 r_p p & p \geq 80 \end{cases} \tag{3}$$

where $\delta\mathbf{p}$ is the phase correction to be applied to the subpixel center of brightness, $\hat{\mathbf{s}}$ is the incoming Sun unit vector in the image, r_p is the apparent radius of the body in pixels, and p is the phase angle in degrees.[16]

Resolved Optical Navigation. As the spacecraft approaches its target, the target begins to grow in the field of view until it subtends many pixels and is no longer dominated by the point spread function of the camera. At this point, more advanced techniques are required to find the center-of-figure in each image. In GIANT, there are numerous techniques for handling resolved bodies, including moment algorithms,[14] template matching,[14] limb matching,[17] and surface feature navigation.[18]

Moment Algorithms. The simplest step up from unresolved OpNav is using a moment algorithm to find the center of brightness of a target and then correcting for the phase angle between the viewing direction and the illumination direction. In GIANT, the moment algorithm is implemented just as a center-of-mass algorithm:

$$\mathbf{x}_b = \frac{\sum_i \mathbf{x}_i * I_i}{\sum_i I_I} \tag{4}$$

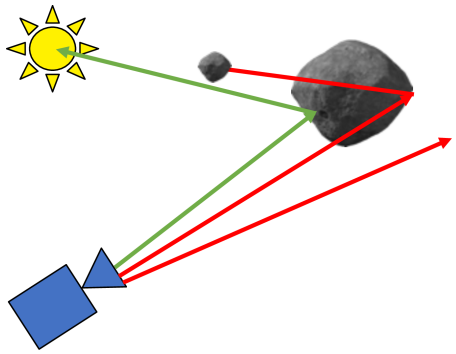

Figure 1. A graphical depiction of a SBRT. The ray in green is illuminated. The rays in red are either shadowed or do not strike the surface so they are not illuminated.

where $\mathbf{x}_b$ is the center of brightness of the target in the image, $\mathbf{x}_i$ is the i^{th} pixel containing the illuminated portion of the target, and I_i is the DN value in $\mathbf{x}_i$. The pixels containing the target are determined by using Otsu's method to extract the target from the background.[19] Once the center of brightness of the target in the image is determined, it is corrected for the phase angle using the same formula as for unresolved OpNav in Eq. (3).[16]

Template Matching. Template matching refers to the process of identifying the location within a full image that matches a smaller template.[20] Traditionally, in computer-vision applications, this is done by comparing two actual images, one of the object of interest by itself, and one where the object of interest is somewhere inside of a larger scene containing many objects. In OpNav, however, we typically "render" our template based upon our *a priori* knowledge of where the camera was when it took an image and what we think the target looks like according to a shape and illumination model.[14] This rendered template is then located in the image using the same techniques as in computer vision, normally through normalized cross-correlation.

In GIANT, the template rendering is handled through the use of a single-bounce ray tracer (SBRT) and a bi-directional reflectance distribution function (BRDF). The SBRT traces a ray from the camera through a scene to the target being considered as shown in Fig. 1. The steps to perform the SBRT and render a template are:

1. Determine the pixels, $\mathbf{p}$, in the image that are expected to contain the target by projecting the bounding box or bounding ellipsoid of the target's shape model onto the image using the *a priori* knowledge of the relative position and orientation between the camera and the target.
    (a) If the predicted location of the target is fully outside the field of view of the camera, temporarily recenter the target at the boresight of the camera for rendering purposes and return to step 1.
2. For each pixel $\mathbf{p}_i$ in $\mathbf{p}$, sample n subpixel locations, $\mathbf{p}_{ij}$, $j \in 1 \dots n$, inside the pixel to be traced through the scene.
3. For each $\mathbf{p}_{ij}$, determine the ray $\mathbf{r}_{ij}$ along the line of sight that projects onto the subpixel point using the inverse camera model.
4. Trace each $\mathbf{r}_{ij}$ through the scene to see if it strikes the target shape model.
    (a) If $\mathbf{r}_{ij}$ strikes the target, store the intersection point, surface normal of the shape model at the intersection point, albedo of the shape model at the intersection point, and direction to the light source from the intersection point, and then "bounce" the ray from the intersection point toward the light source (Sun).
        i. If the bounced ray does not strike any other portion of the target shape model, or any other objects contained in the scene before it reaches the light source, then that ray is visible and the stored geometry of the observation is provided to the BRDF being used to compute an illumination value for that ray resulting in an illumination value I_{ij}.
        ii. If the bounced ray strikes another portion of the target shape model, or any other objects contained in the scene before it reaches the light source, then set the illumination value $I_{ij} = 0$.
    (b) If $\mathbf{r}_{ij}$ does not strike the target, set the illumination for that ray equal to 0, $I_{ij} = 0$.
5. Sum the illumination values for every ray $\mathbf{r}_{ij}$ in pixel $\mathbf{p}_i$ to compute the illumination value for the pixel.
6. Repeat steps 2–5 until the illumination values have been computed for all pixels containing the predicted location of the target.

The end result is a rendered template that can then be identified in the image. The shape models in GIANT can be constructed from triangles, parallelograms, or triaxial ellipsoids. Shape models constructed from a large number of triangles or parallelograms can be placed into a KDTree object to allow for more efficient ray tracing.[21]

With the rendered template it is now possible to identify the location of the target in the image. In GIANT, this is done using normalized cross-correlation.[14] The normalized cross-correlation produces a correlation matrix with values between -1 and 1. The peak of the correlation matrix corresponds to the location in the image where the template best matches the image. This correlation surface around the peak can be fit with a 2D parabaloid in a least squares sense to get the subpixel

peak of the correlation surface. Accounting for the location of the center-of-figure of the target in the template allows for the correlation peak to be directly related to the observed center-of-figure of the target in the image.

In cases where there may be a range error in the *a priori* knowledge of the relative position between the camera and the target, or when there may be a scale error in the knowledge of the overall size of the shape of the target, the usual cross-correlation routines can begin to become biased due to differences in the template and the actual image. Therefore, GIANT also provides an alternative template matching technique, as described in Ref. [22].

Limb Matching. In limb matching, observed limb points from the image are matched to predicted limb points from the shape model of the target object and are used to identify either the center-of-figure of the target in the image[14] or the full 3-degree-of-freedom relative position between the camera and the target.[17,23] Essentially, the procedures follow a basic pattern:

1. Identify limb points in the image using edge detection[24] or limb-scanning.[14]

2. Match the limb points from the image with predicted limb points from a shape model of the target.[14,17,23]

3. Estimate either an update[14,17] to or the final solution[23] for the center-of-figure of the target in the image or the full 3-degree-of-freedom relative position between the camera and the target depending on the technique being used.

GIANT provides routines to perform limb matching for both regular and irregular bodies directly as described in Refs. [17, 23].

Surface Feature Navigation. Surface feature navigation refers to the process of identifying surface features or small patches of a surface in an image of a target.[2,18] GIANT provides routines to perform surface feature navigation using similar steps to those described in the template matching section. More details are provided in Ref. [18].

Results. GIANT has been successfully used to support the IV&V orbit determination efforts throughout proximity operations at asteroid Bennu. The following results show the results from each set of algorithms.

Camera Calibration. During the cruise phase of the mission, multiple calibration campaigns were undertaken to perform geometric and photometric calibration of the imagers on OSIRIS-REx.[25] In this subsection we briefly present the results of the geometric camera calibration performed using GIANT for each camera used for OpNav,[26,27] along with the post-fit residuals of the stars used to perform the calibration.

For each calibration, the following model was used to perform the fit[11]

$$\mathbf{x}_I = \frac{1}{z_C}\begin{bmatrix} x_C \\ y_C \end{bmatrix} \tag{5}$$

$$r = \sqrt{x_I^2 + y_I^2} \tag{6}$$

$$\Delta\mathbf{x}_I = (k_1 r^2 + k_2 r^4 + k_3 r^6)\mathbf{x}_I + \begin{bmatrix} 2p_1 x_I y_I + p_2(r^2 + 2x_I^2) \\ p_1(r^2 + 2y_I^2) + 2p_2 x_I y_I \end{bmatrix} \tag{7}$$

$$\mathbf{x}_P = \begin{bmatrix} f_x & 0 & c_x \\ 0 & f_y & c_y \end{bmatrix} \begin{bmatrix} (1 + a_1 T)(\mathbf{x}_I + \Delta\mathbf{x}_I) \\ 1 \end{bmatrix} \tag{8}$$

where $\mathbf{x}_C = \begin{bmatrix} x_C & y_C & z_C \end{bmatrix}^T$ is a point expressed in the camera frame, $\mathbf{x}_I$ is the image frame coordinate for the point (pinhole location), r is the radial distance from the principal point of the camera to the gnomic location of the point, k_{1-3} are radial distortion coefficients, p_{1-2} are tip/tilt/prism distortion coefficients, $\Delta\mathbf{x}_I$ is the distortion for point $\mathbf{x}_I$, f_x and f_y are the focal length divided by the pixel pitch in the x and y directions respectively expressed in units of pixels, c_x and c_y are the location of the principal point of the camera in the image expressed in units of pixels, T is the temperature of the camera, a_1 is the temperature dependence coefficient, and $\mathbf{x}_P$ is the pixel location of the point in the image. In addition, the UCAC4 star catalogue[28] was used to provide the "truth" star locations for the calibration. Table 1 shows the results of the geometric camera calibration for each camera while Figs. 2–6 show the post-fit residuals from the calibration procedure. The post-fit residuals of the camera calibration are all near 0.1 pixels in standard deviation, which is approximately the accuracy of the sub-pixel center of brightness routine used to identify the star locations in the image, and are largely random without structure, indicating that the calibrations successfully modeled the camera and the errors are due to the image processing.

Approach. During Approach to Bennu in late 2018, OpNav provided the initial acquisition of Bennu. Throughout this phase, Bennu grew from much less than 1 pixel to greater than 1000 pixels in apparent diameter and most of the imaging was handled by the PolyCam and MapCam imagers.[26] In addition, the traditional OpNav cadence of short/long-exposure pairs was used to both perform attitude estimation and relative navigation with respect to Bennu.[29]

Figs. 7 and 8 show the post-fit star residuals from the attitude estimation in GIANT. The residuals are around 0.1 pixels, showing the quality of the attitude estimates and the camera model that was used.

Figs. 9 and 10 show both the unresolved and cross-correlation center-finding results from processing the short OpNav images with GIANT. The residuals are

Table 1. Geometric camera models as estimated by GIANT.

	f_x	f_y	c_x	c_y	k_1	k_2	k_3	p_1	p_2	a_1
PolyCam	73881.8	-73890.1	511.5*	511.5*	13.761	0*	0*	2.38e-4	-6.90e-4	0*
MapCam Pan	14737.0	-14736.5	511.5*	511.5*	0.967	0*	0*	-3.77e-3	1.20e-3	-2.22e-5
MapCam V	14719.9	-14620.3	511.5*	511.5*	0.952	0*	0*	-3.99e-3	1.09e-3	1.06e-5
NavCam 1	3473.3	-3473.4	1268.7	949.6	-0.539	0.388	-0.214	-2.55e-4	8.64e-4	2.37e-5
NavCam2	3462.6	-3462.6	1309.7	968.3	-0.539	0.389	-0.219	6.00e-4	-1.34e-4	1.97e-5

* Not estimated

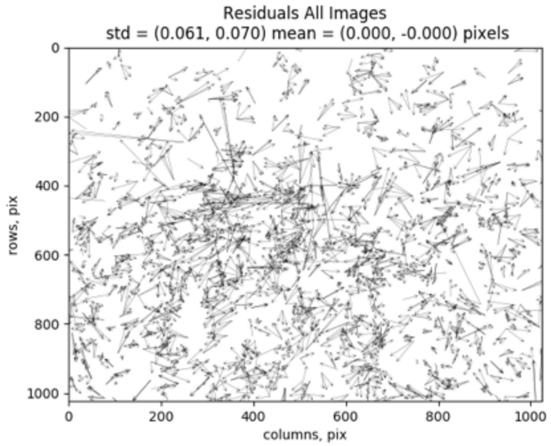

Figure 2. The post-fit residuals from performing the geometric camera calibration for the PolyCam camera with the OpNav focus set.

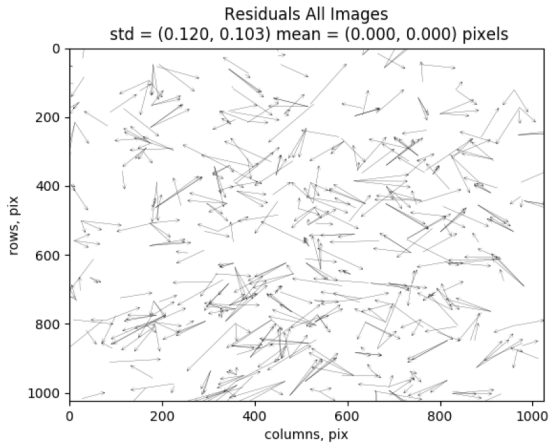

Figure 4. The post-fit residuals from performing the geometric camera calibration for the MapCam camera with the V filter.

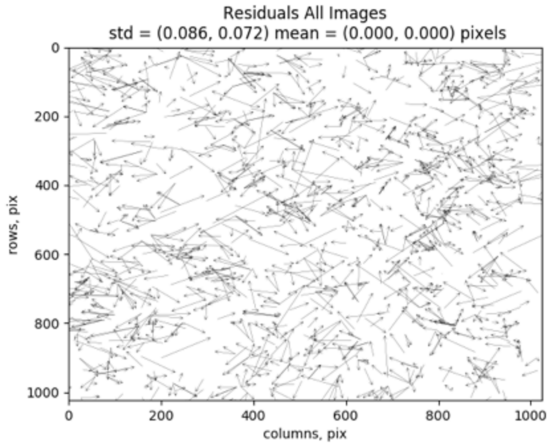

Figure 3. The post-fit residuals from performing the geometric camera calibration for the MapCam camera with the Pan filter.

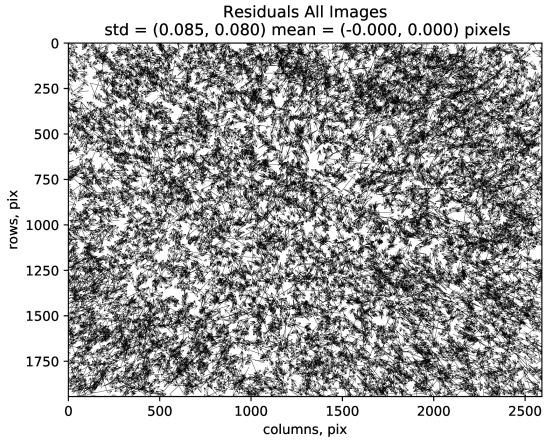

Figure 5. The post-fit residuals from performing the geometric camera calibration for the NavCam 1 camera.

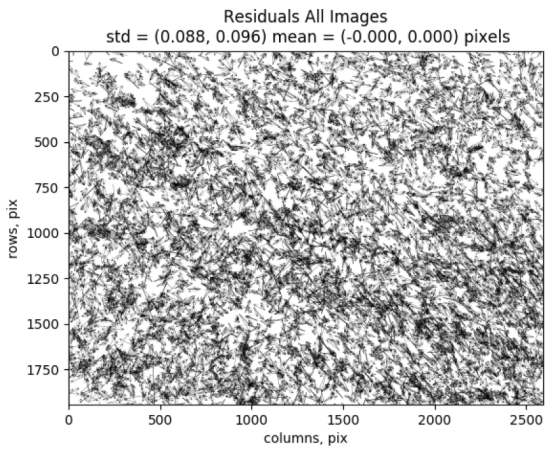

Figure 6. The post-fit residuals from performing the geometric camera calibration for the NavCam2 camera.

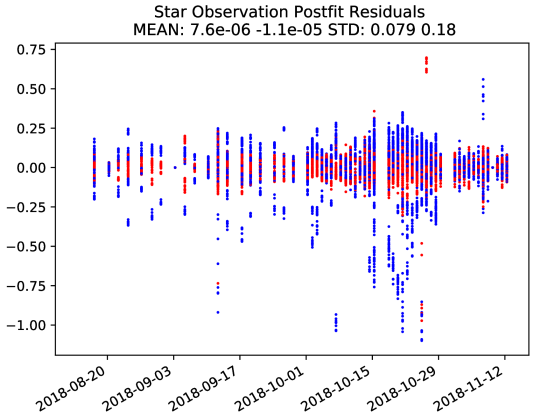

Figure 7. The post-fit star residuals from performing the attitude estimation on star images taken using PolyCam during Approach.

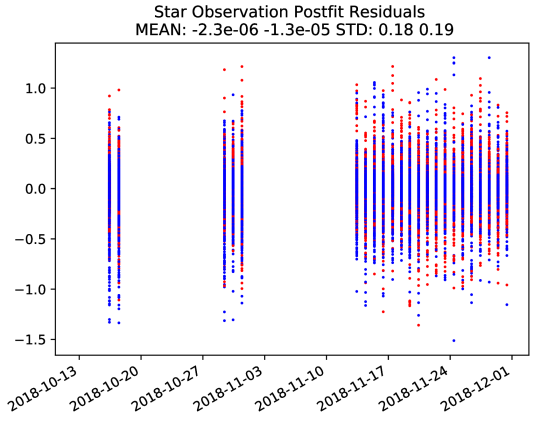

Figure 8. The post-fit star residuals from performing the attitude estimation on star images taken using MapCam during Approach.

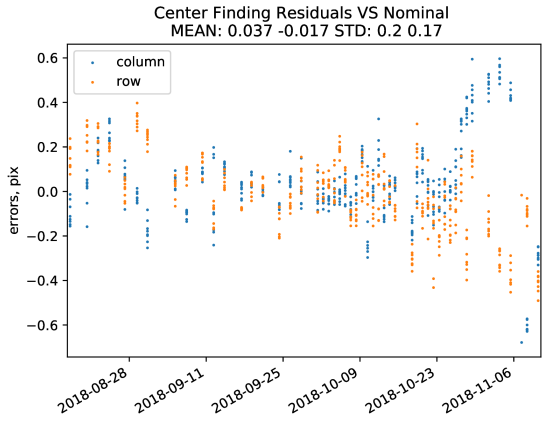

Figure 9. The post-fit center-finding OpNav residuals from images taken by PolyCam during Approach. The residuals are between the observed location found in GIANT and the expected location based on the best-fit trajectory for OSIRIS-REx and Bennu from the IV&V OD processes.

typically less than 1 pixel, which is as expected and shows that the GIANT solutions fit well in the OD solutions produced by the IV&V team.

Finally, Figs. 11-14 show the center-finding and range results from the limb-based algorithms. The residuals are excellent for the center-finding and the range estimates are less than 1% of the total range, which is the expected performance.

For the cross-correlation and limb-based navigation algorithms, we used the final shape model that was produced based on the Approach imaging.

Preliminary Survey. During Preliminary Survey in December 2018, OSIRIS-REx made multiple flybys of Bennu in order to get global coverage of the surface of Bennu. Throughout this phase, Bennu was approximately 100-250 pixels in apparent diameter and most of the imaging was done using the NavCam 1 imager.[27] In addition, the traditional OpNav cadence of short/long-exposure pairs was used to both perform attitude estimation and relative navigation with respect to Bennu.

Figs. 15 and 16 show the post-fit star residuals from the attitude estimation in GIANT. The residuals are around 0.1 pixels, showing the quality of the attitude estimates and the camera model that was used.

Figs. 17 and 18 show the cross-correlation center-finding results from processing the short OpNav images with GIANT. The residuals are typically less than 1 pixel, which is as expected and shows that the GIANT solutions fit well in the OD solutions produced by the IV&V team.

Finally, Figs. 19–22 show the center-finding and range results from the limb-based algorithms. The residuals are excellent for the center-finding and the range esti-

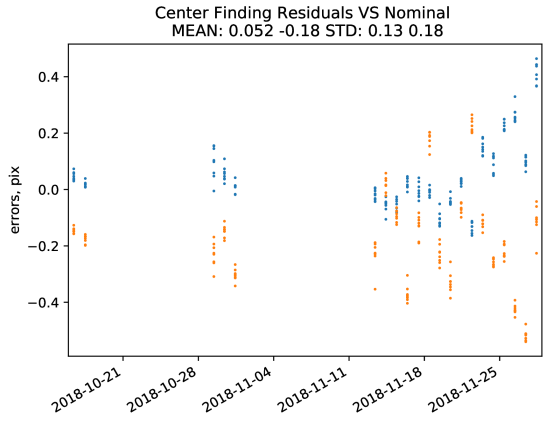

Figure 10. The post-fit center-finding OpNav residuals from images taken by MapCam during Approach. The residuals are between the observed location found in GIANT and the expected location based on the best-fit trajectory for OSIRIS-REx and Bennu from the IV&V OD processes.

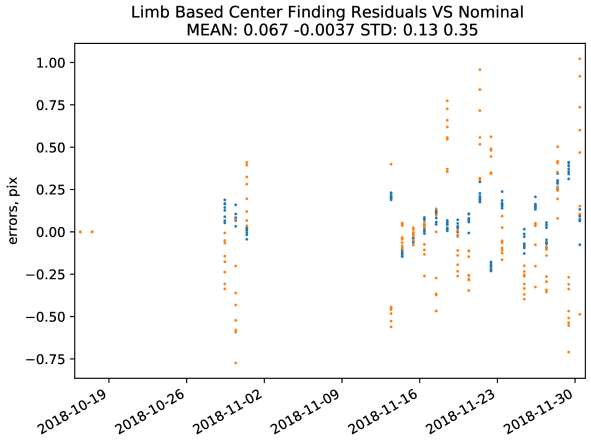

Figure 12. The post-fit center-of-figure OpNav residuals from images taken by MapCam during Approach using the limb-based OpNav technique. The residuals are between the observed location found in GIANT and the expected location based on the best-fit trajectory for OSIRIS-REx and Bennu from the IV&V OD processes.

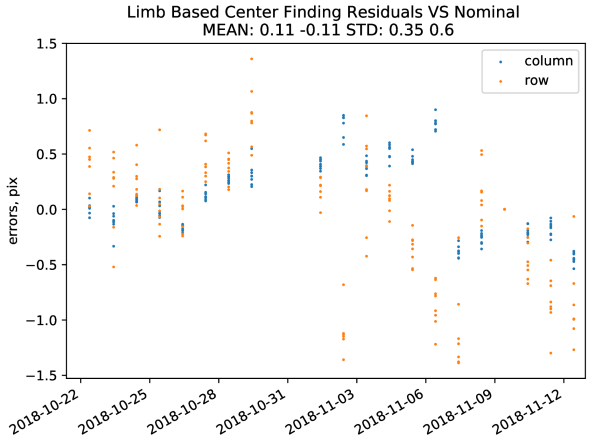

Figure 11. The post-fit center-of-figure OpNav residuals from images taken by PolyCam during Approach using the limb-based OpNav technique. The residuals are between the observed location found in GIANT and the expected location based on the best-fit trajectory for OSIRIS-REx and Bennu from the IV&V OD processes.

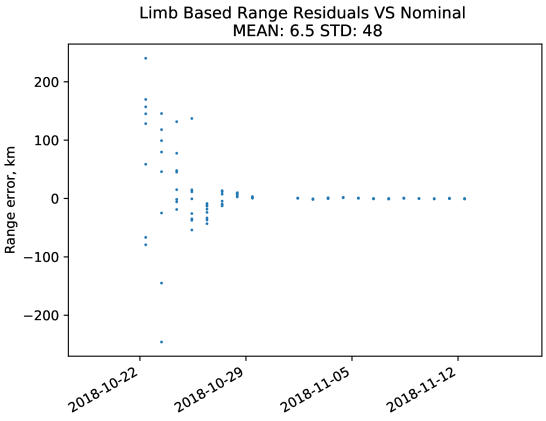

Figure 13. The post-fit range residuals from images taken by PolyCam during Approach using the limb-based OpNav technique. The residuals are between the observed range found in GIANT and the expected range based on the best-fit trajectory for OSIRIS-REx and Bennu from the IV&V OD processes.

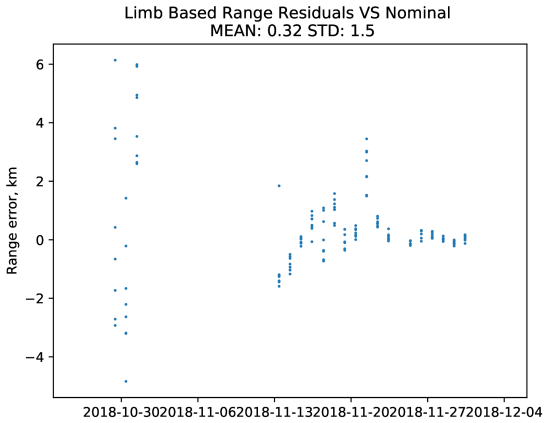

Figure 14. The post-fit range residuals from images taken by MapCam during Approach using the limb-based OpNav technique. The residuals are between the observed range found in GIANT and the expected range based on the best-fit trajectory for OSIRIS-REx and Bennu from the IV&V OD processes.

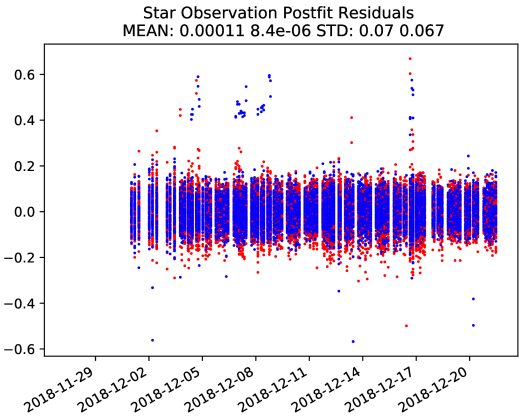

Figure 16. The post-fit star residuals from performing the attitude estimation on star images taken using NavCam 1 during Preliminary Survey.

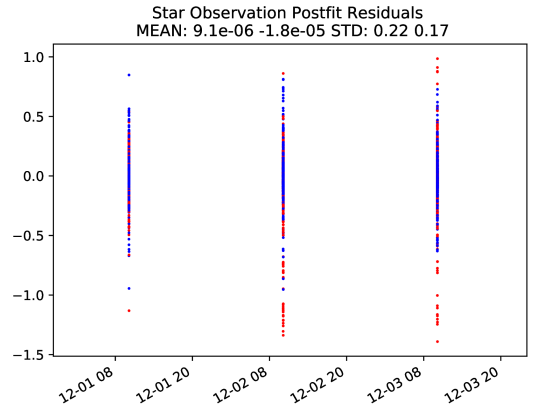

Figure 15. The post-fit star residuals from performing the attitude estimation on star images taken using MapCam during Preliminary Survey.

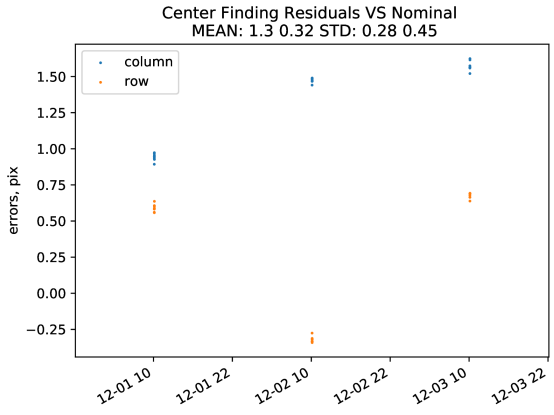

Figure 17. The post-fit center-finding OpNav residuals from images taken by MapCam during Preliminary Survey. The residuals are between the observed location found in GIANT and the expected location based on the best-fit trajectory for OSIRIS-REx and Bennu from the IV&V OD processes.

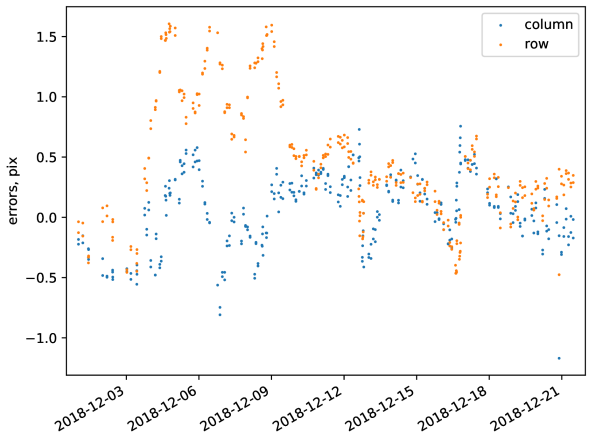

Figure 18. The post-fit center-finding OpNav residuals from images taken by NavCam 1 during Preliminary Survey. The residuals are between the observed location found in GIANT and the expected location based on the best-fit trajectory for OSIRIS-REx and Bennu from the IV&V OD processes.

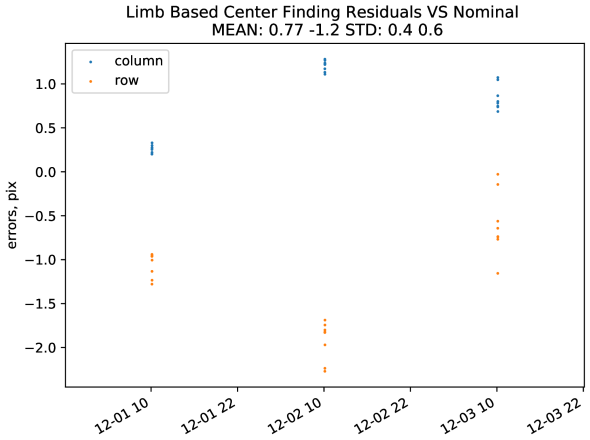

Figure 19. The post-fit center-of-figure OpNav residuals from images taken by MapCam during Preliminary Survey using the limb-based OpNav technique. The residuals are between the observed location found in GIANT and the expected location based on the best-fit trajectory for OSIRIS-REx and Bennu from the IV&V OD processes.

mates are less than 0.01% of the total range, which is the expected performance.

For the cross-correlation and limb-based navigation algorithms, we used the final shape model that was produced based on the Preliminary Survey imaging.

Orbital A. During Orbital A in Winter 2019, OSIRIS-REx entered into a frozen polar terminator orbit that was about 1.5 km in radius in order to transition from center-finding to surface feature navigation using SPC. Throughout this phase, Bennu was approximately 1000 pixels in apparent diameter and all of the navigation imaging was done using the NavCam 1 imager. In addition, the traditional OpNav cadence of short/long-exposure pairs was used to both perform attitude estimation and relative navigation with respect to Bennu.

Fig. 23 shows the post-fit star residuals from the attitude estimation in GIANT. The residuals are less than 0.1 pixels.

Fig. 24 shows the cross-correlation center-finding results from processing the short OpNav images with GIANT. The residuals are typically less than 1 pixel, which is as expected and shows that the GIANT solutions fit well in the OD solutions produced by the IV&V team.

Finally, Figs. 25 and 26 show the center-finding and range results from the limb-based algorithms. The residuals are excellent for the center-finding and the range estimates are less than 0.01% of the total range, which is the expected performance.

For the cross-correlation and limb-based navigation algorithms, we used the final shape model that was produced based on the Preliminary Survey imaging.

Detailed Survey. During Detailed Survey in spring 2019, OSIRIS-REx again performed multiple flybys to

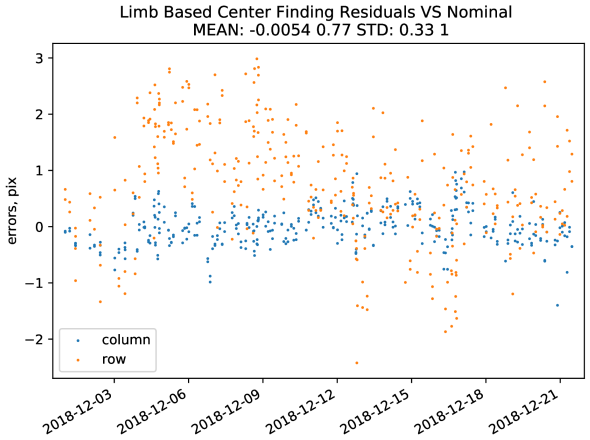

Figure 20. The post-fit center-of-figure OpNav residuals from images taken by NavCam during Preliminary Survey using the limb-based OpNav technique. The residuals are between the observed location found in GIANT and the expected location based on the best-fit trajectory for OSIRIS-REx and Bennu from the IV&V OD processes.

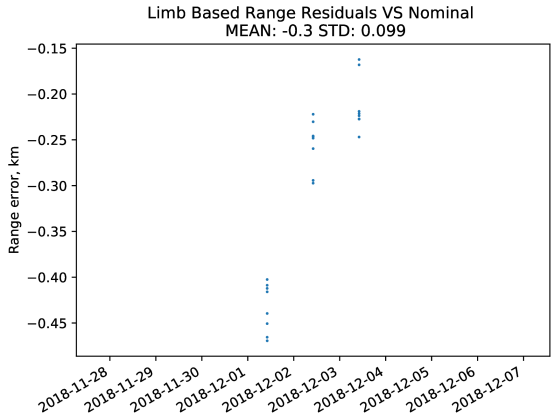

Figure 21. The post-fit range residuals from images taken by MapCam during Preliminary Survey using the limb-based OpNav technique. The residuals are between the observed range found in GIANT and the expected range based on the best-fit trajectory for OSIRIS-REx and Bennu from the IV&V OD processes.

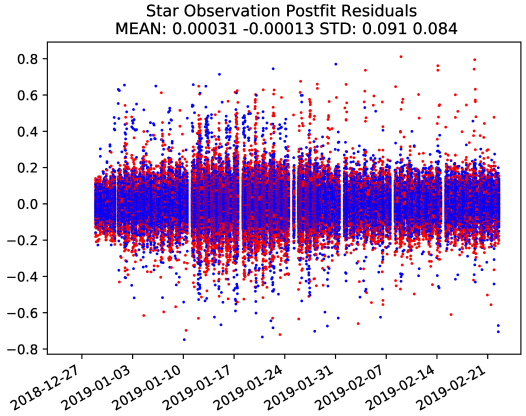

Figure 23. The post-fit star residuals from performing the attitude estimation on star images taken using NavCam 1 during Orbital A.

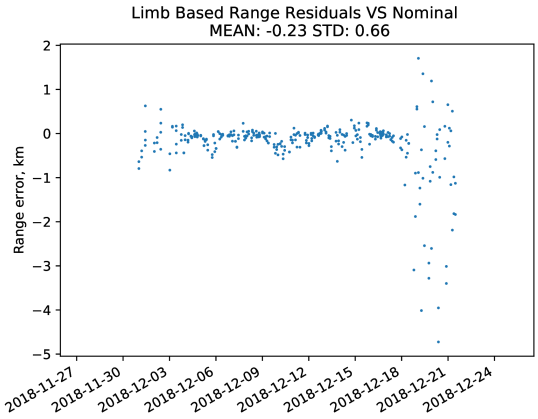

Figure 22. The post-fit range residuals from images taken by NavCam 1 during Preliminary Survey using the limb-based OpNav technique. The residuals are between the observed range found in GIANT and the expected range based on the best-fit trajectory for OSIRIS-REx and Bennu from the IV&V OD processes.

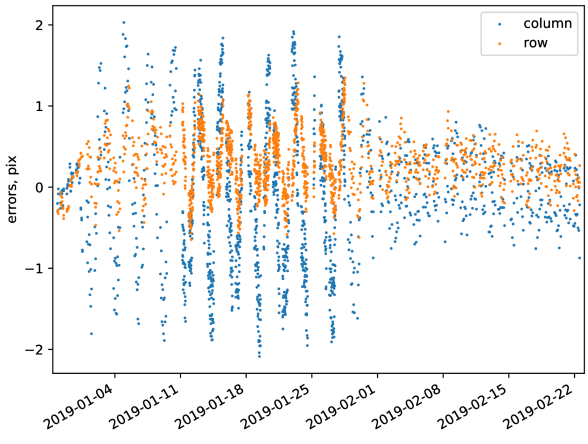

Figure 24. The post-fit center-finding OpNav residuals from images taken by NavCam 1 during Orbital A. The residuals are between the observed location found in GIANT and the expected location based on the best-fit trajectory for OSIRIS-REx and Bennu from the IV&V OD processes.

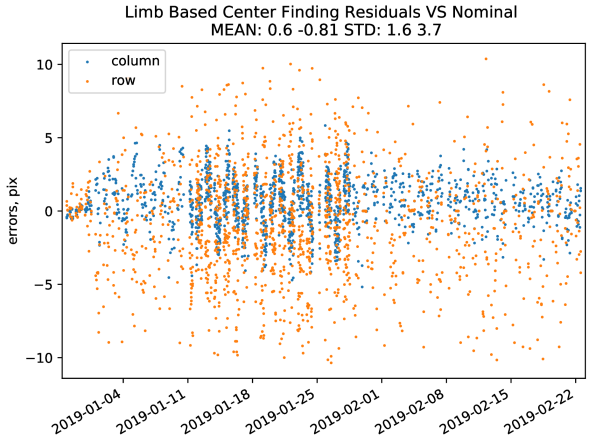

Figure 25. The post-fit center-of-figure OpNav residuals from images taken by NavCam during Orbital A using the limb-based OpNav technique. The residuals are between the observed location found in GIANT and the expected location based on the best-fit trajectory for OSIRIS-REx and Bennu from the IV&V OD processes.

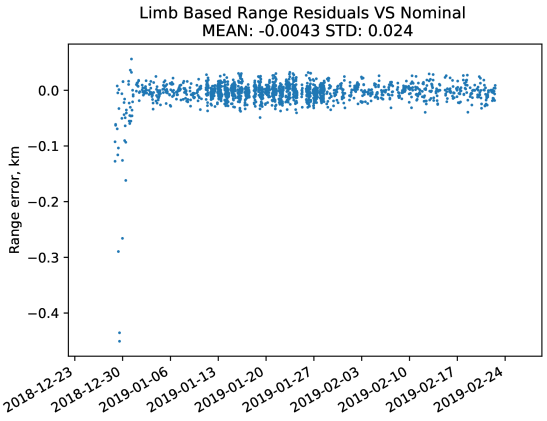

Figure 26. The post-fit range residuals from images taken by NavCam 1 during Orbital A using the limb-based OpNav technique. The residuals are between the observed range found in GIANT and the expected range based on the best-fit trajectory for OSIRIS-REx and Bennu from the IV&V OD processes.

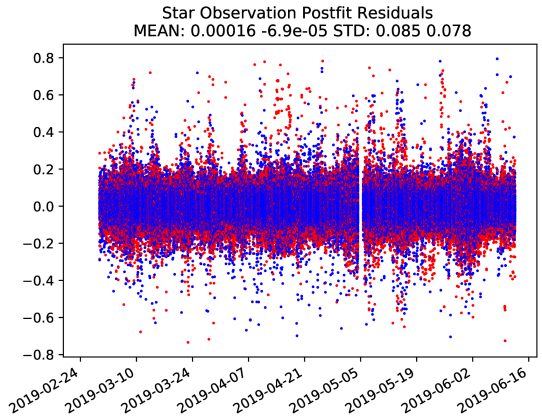

Figure 27. The post-fit star residuals from performing the attitude estimation on star images taken using NavCam 1 during Detailed Survey.

get higher-resolution global coverage of Bennu's surface. Throughout this phase, Bennu was approximately 200-600 pixels in apparent diameter in NavCam 1 and larger than the field of view in MapCam. In addition, the traditional OpNav cadence of short/long-exposure pairs was used to perform attitude estimation and relative navigation with respect to Bennu for NavCam 1, while only short exposure images were captured using MapCam. Because Bennu filled the field of view of MapCam, star-based attitude estimation, and center-finding/limb-based OpNav is not possible, therefore we do not consider the MapCam images in this section.

Fig. 27 shows the post-fit star residuals from the attitude estimation in GIANT. The residuals are around 0.1 pixels, showing the quality of the attitude estimates and the camera model that was used.

Fig. 28 shows the cross-correlation center-finding results from processing the short OpNav images with GIANT. The residuals are typically less than 1 pixel, which is as expected and shows that the GIANT solutions fit well in the OD solutions produced by the IV&V team.

Finally, Figs. 29–30 show the center-finding and range results from the limb-based algorithms. The residuals are excellent for the center-finding and the range estimates are less than 0.01% of the total range, which is the expected performance.

For the cross-correlation and limb-based navigation algorithms, we used the final shape model that was produced based on the Detailed Survey imaging.

Conclusion. The GIANT tool has been successfully used to perform IV&V Optical Navigation on OSIRIS-REx. The results demonstrate the quality of the GIANT measurements and their use in performing orbit determination about a small body. Future work includes performance improvements and implementation of new cutting-edge OpNav algorithms to ensure GIANT re-

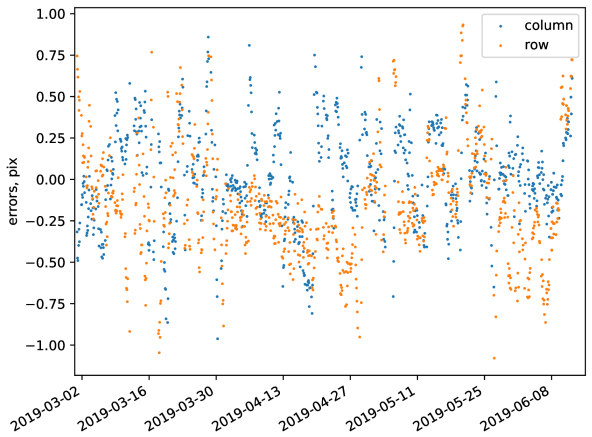

Figure 28. The post-fit center-finding OpNav residuals from images taken by NavCam 1 during Detailed Survey. The residuals are between the observed location found in GIANT and the expected location based on the best-fit trajectory for OSIRIS-REx and Bennu from the IV&V OD processes.

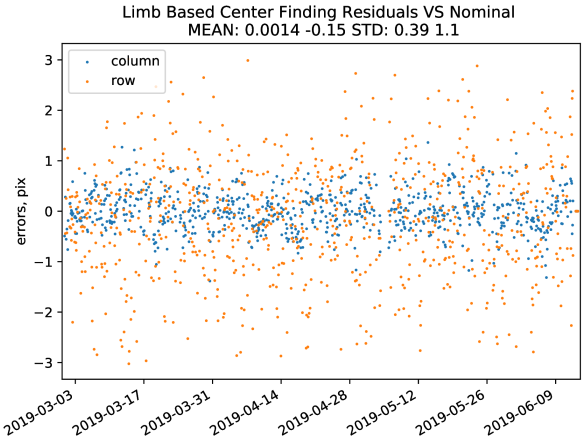

Figure 29. The post-fit center-of-figure OpNav residuals from images taken by NavCam during Detailed Survey using the limb-based OpNav technique. The residuals are between the observed location found in GIANT and the expected location based on the best-fit trajectory for OSIRIS-REx and Bennu from the IV&V OD processes.

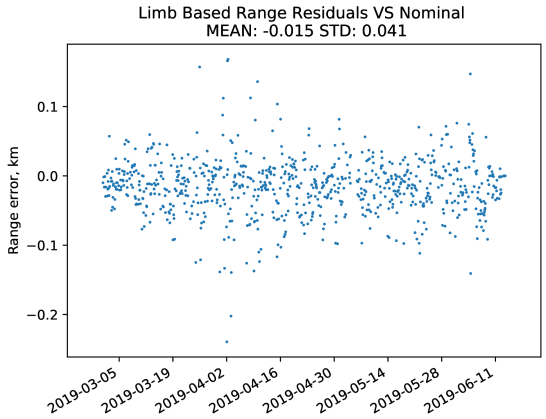

Figure 30. The post-fit range residuals from images taken by NavCam 1 during Detailed Survey using the limb-based OpNav technique. The residuals are between the observed range found in GIANT and the expected range based on the best-fit trajectory for OSIRIS-REx and Bennu from the IV&V OD processes.

mains capable of performing OpNav for a wide range of missions.

Acknowledgments. The authors are grateful to the entire OSIRIS-REx Team for making the encounter with Bennu possible. They would also like to thank Natalie Liounis and Cat Wolner for their assistance in preparing this document. This material is based upon work supported by NASA under Contracts NNM10AA11C and NNG13FC02C issued through the New Frontiers Program.

References.

[1] J. L. Geeraert, J. M. Leonard, P. W. Kenneally, P. G. Antreasian, M. C. Moreau, and D. S. Lauretta, "OSIRIS-REx Navigation Small Force Models," in *Astrodynamics Specialist Conference*, AIAA, 2019.

[2] R. Gaskell, O. Barnouin-Jha, D. Scheeres, A. Konopliv, T. Mukai, S. Abe, J. Saito, M. Ishiguro, T. Kubota, T. Hashimoto, J. Kawaguchi, M. Yoshikawa, K. Shirakawa, T. Kominato, N. Hirata, and H. Demura, "Characterizing and navigating small bodies with imaging data," *Meteoritics & Planetary Science*, vol. 43, no. 6, pp. 1049–1061, 2008. doi: 10.1111/j.1945-5100.2008.tb00692.x.

[3] D. Lang, D. W. Hogg, K. Mierle, M. Blanton, and S. Roweis, "Astrometry.net: Blind Astrometric Calibration of Arbitrary Astronomical Images," *The Astronomical Journal*, vol. 139, no. 5, p. 1782, 2010.

[4] K. G. Derpanis, "Overview of the RANSAC Algorithm," tech. rep., Department of Electrical Engineering and Computer Science, York University.

[5] J. A. Christian, L. Benhacine, J. Hikes, and C. DâĂŹSouza, "Geometric Calibration of the Orion Optical Navigation Camera Using Star Field Images," *The Journal of the Astronautical Sciences*, vol. 63, no. 4, pp. 335–353, 2016.

[6] A. J. Liounis, J. L. Small, J. C. Swenson, J. R. Lyzhoft, B. W. Ashman, K. M. Getzandanner, M. C. Moreau, C. D.

Adam, J. M. Leonard, D. S. Nelson, J. Y. Pelgrift, B. J. Bos, S. R. Chesley, C. W. Hergenrother, and D. S. Lauretta, "Autonomous Detection of Particles and Tracks in Optical Images," *Earth and Space Science*, 2020.

[7] L. Di Stefano and A. Bulgarelli, "A Simple and Efficient Connected Components Labeling Algorithm," in *Proceedings 10th International Conference on Image Analysis and Processing*, pp. 322–327, 1999.

[8] G. Wahba, "A least squares estimate of satellite attitude," *SIAM review*, vol. 7, no. 3, pp. 409–409, 1965.

[9] P. B. Davenport, "A vector approach to the algebra of rotations with applications," Tech. Rep. NASA-TM-X-57187, NASA Goddard Space Flight Center, 1968.

[10] J. A. Christian, L. Benhacine, J. Hikes, and C. D'Souza, "Geometric calibration of the orion optical navigation camera using star field images," *The Journal of the Astronautical Sciences*, vol. 63, pp. 335–353, Dec 2016.

[11] D. C. Brown, "Decentering distortion of lenses," *Photogrammetric Engineering and Remote Sensing*, vol. 32, no. 3, 1966.

[12] OpenCV Team, "Camera calibration and 3d reconstruction." `https://docs.opencv.org/master/d9/d0c/group__calib3d.html`, 2019.

[13] P. Sturm, "Pinhole camera model," *Computer Vision: A Reference Guide*, pp. 610–613, 2014.

[14] W. M. Owen Jr., "Methods of Optical Navigation," in *21st Annual AAS/AIAA Space Flight Mechanics Meeting*, (New Orleans), AAS, 2011.

[15] C. Jackman and P. Dumont, "Optical Navigation Capabilities for Deep Space Missions," in *Proceedings of the 23rd AAS/AIAA Space Flight Mechanics Conference*, 2013.

[16] M. Kaasalainen and P. Tanga, "Photocentre offset in ultra-precise astrometry: Implications for barycentre determination and asteroid modelling," *Astronomy & Astrophysics*, vol. 416, no. 1, pp. 367–373, 2004.

[17] A. J. Liounis, "Limb Based Optical Navigation for Irregular Bodies," in *1st Annual RPI Workshop on Image-Based Modeling and Navigation for Space Applications, Troy, NY*, 2018.

[18] C. R. Gnam, B. W. Ashman, and A. J. Liounis, "A Novel Surface Feature Navigatio Algorithm Using Ray Tracing," in *2nd RPI Space Imaging Workshop, Saratoga Springs, NY*, 2019.

[19] N. Otsu, "A threshold selection method from gray-level histograms," *IEEE Transactions on Systems, Man, and Cybernetics*, vol. 9, no. 1, pp. 62–66, 1979.

[20] R. Brunelli, *Template Matching Techniques in Computer Vision: Theory and Practice*. John Wiley & Sons, 2009.

[21] M. Hapala and V. Havran, "Review: Kd-tree traversal algorithms for ray tracing," *Computer Graphics Forum*, vol. 30, no. 1, pp. 199–213, 2011.

[22] J. R. Lyzhoft, A. J. Liounis, C. D. Adam, P. G. Antreasian, and D. S. Lauretta, "Template Matching Used for Small Body Optical Navigation with Poorly Detailed Objects," in *2nd RPI Space Imaging Workshop, Saratoga Springs, NY*, 2019.

[23] J. A. Christian, "Accurate planetary limb localization for image-based spacecraft navigation," *Journal of Spacecraft and Rockets*, pp. 1–23, 2017.

[24] A. Trujillo-Pino, K. Krissian, M. AlemÃąn-Flores, and D. Santana-CedrÃĺs, "Accurate subpixel edge location based on partial area effect," *Image and Vision Computing*, vol. 31, no. 1, pp. 72 – 90, 2013.

[25] J. Y. Pelgrift, E. M. Sahr, D. S. Nelson, C. D. Jackman, L. Benhacine, B. J. Bos, B. Rizk, C. D. dâĂŹAubigny, D. R. Golish, D. N. Dellagiustina, and D. S. Lauretta, "In-Flight Calibration of the OSIRIS-REx Optical Navigation Imagers," in *1st Annual RPI Workshop on Image-Based Modeling and Navigation for Space Applications, Troy, NY*, 2018.

[26] B. Rizk, C. D. dâĂŹAubigny, D. Golish, C. M. Fellows, C. Merrill, P. Smith, M. S. Walker, J. E. Hendershot, J. Hancock, S. Bailey, D. N. DellaGiustina, D. S. Lauretta, R. D. Tanner, M. Williams, K. Harshman, M. Fitzgibbon, W. Verts, J. Chen, T. Connors, D. Hamara, A. Dowd, A. Lowman, M. B. Dubin, R. Burt, M. Whiteley, M. F. Watson, T. J. McMahon, M. Ward, D. Booher, M. S. Read, B. Williams, M. Hunten, E. Little, T. Saltzman, D. Alfred, S. OâĂŹDougherty, M. Walthall, K. Kenagy, S. Peterson, B. Crowther, M. Perry, C.-T. See, S. Selznick, C. Sauve, M. Beiser, W. J. Black, R. N. Pfisterer, A. Lancaster, S. Oliver, C. Oquest, D. Crowley, C. Morgan, C. Castle, R. Domínguez, and M. Sullivan, "OCAMS: The OSIRIS-REx Camera Suite," *Space Science Reviews*, vol. 214, pp. 1–55, 2018.

[27] B. Bos, M. Ravine, M. Caplinger, J. Schaffner, J. Ladewig, R. Olds, C. Norman, D. Huish, M. Hughes, S. Anderson, *et al.*, "Touch and Go Camera System (TAGCAMS) for the OSIRIS-REx asteroid sample return mission," *Space Science Reviews*, vol. 214, no. 1, p. 37, 2018.

[28] N. Zacharias, C. Finch, T. Girard, A. Henden, J. Bartlett, D. Monet, and M. Zacharias, "The Fourth US Naval Observatory CCD Astrograph Catalog (UCAC4)," *The Astronomical Journal*, vol. 145, no. 2, p. 44, 2013.

[29] C. D. Jackman, D. S. Nelson, L. K. Mccarthy, T. J. Finley, A. J. Liounis, K. M. Getzandanner, P. G. Antreasian, and M. C. Moreau, "Optical Navigation Concept of Operations for the Osiris-Rex Mission," in *AAS/AIAA Spaceflight Mechanics Meeting*, pp. 1–18, 2017.